Journal of Nuclear Materials 389 (2009) 149–154

Contents lists available at ScienceDirect

Journal of Nuclear Materials

journal homepage: www.elsevier.com/locate/jnucmat

Evaluation of melting point of UO_2 by molecular dynamics simulation

Tatsumi Arima [a,*], Kazuya Idemitsu [a], Yaohiro Inagaki [a], Yuichi Tsujita [b], Motoyasu Kinoshita [c], Eugene Yakub [d]

[a] Faculty of Engineering, Kyushu University, 744 Motooka, Fukuoka 819-0395, Japan
[b] School of Engineering, Kinki University, 1 Umenobe, Takaya, Higashi-Hiroshima, 739-2116 Hiroshima, Japan
[c] Nuclear Power Department, Central Research Institute of Electric Power Industry, 2-11-1 Iwado-kita, Komae-shi, 201-8511 Tokyo, Japan
[d] Computer Science Department, Odessa State Economic University, 8 Preobrazhenskaya St., 65082 Odessa, Ukraine

ARTICLE INFO

PACS:
28.41.Bm
28.41.Ak
05.70.−a
82.60.−s

ABSTRACT

The melting point of UO_2 has been evaluated by molecular dynamics simulation (MD) in terms of interatomic potential, pressure and Schottky defect concentration. The Born–Mayer–Huggins potentials with or without a Morse potential were explored in the present study. Two-phase simulation whose supercell at the initial state consisted of solid and liquid phases gave the melting point comparable to the experimental data using the potential proposed by Yakub. The heat of fusion was determined by the difference in enthalpy at the melting point. In addition, MD calculations showed that the melting point increased with pressure applied to the system. Thus, the Clausius–Clapeyron equation was verified. Furthermore, MD calculations clarified that an addition of Schottky defects, which generated the local disorder in the UO_2 crystal, lowered the melting point.

1. Introduction

The melting point of uranium dioxide as well as the thermal conductivity is one of the most important properties for the safety management of nuclear fuels. It is well known that UO_2 is exposed to high temperature and irradiation. Such conditions vary widely with position in the fuel, e.g., temperature gradient, high burn-up at the rim region [1], and also vary with loading time, e.g., accumulation of fission products and increase of oxygen partial pressure. As a result, the melting point of uranium oxide is affected by these factors. For example, the melting point of hyper-stoichiometric uranium oxide UO_{2+x} is lower than that of stoichiometric UO_2 [2]. Likewise, the addition of trans-uranium atoms to UO_2 lowers the melting point of fuels [3,4]. So, the effects of Pu and minor actinides should be also investigated systematically to establish the FBR fuel cycle. However, it is somewhat difficult to experimentally evaluate melting points with accuracy since such oxide fuels have very high melting points and radioactive toxicities. As a first step to evaluate the melting points of above fuels, that of UO_2 was estimated by the molecular dynamics (MD) simulation.

MD simulations have ever been used to evaluate the behavior of various thermophysical properties, e.g., thermal expansion, compressibility, specific heat, thermal conductivity, of uranium oxide, plutonium oxide, and mixed uranium–plutonium oxide [5–13] and have shown their usefulness. However, there is little discussion of the melting point in the literature. In general, the melting point obtained from the MD simulation seems to be higher than the experimental one if MD calculations are performed for the homogeneous solid phase at the initial state (one-phase simulation). In order to avoid such misunderstanding, the MD calculation should be performed for the inhomogeneous initial state which consists of solid and liquid phases (so-called the joining two 'boxes' [14] or two-phase simulation [15,16]). More recently, Govers et al. discussed the melting point of UO_2 in terms of an interatomic potential function [14]. They revealed that Karakasidis potential [17] with a rigid ion model gave a melting point comparable to the experimental one.

In the present study, MD calculations were performed using the interatomic potentials with the partially ionic model, i.e. Basak et al. [9], Arima et al. [10] and Yakub et al. [12] potentials. In order to properly assess the melting point, we compared one- and two-phase simulation techniques. The changes in the melting point and the latent heat of melting were investigated as a function of the supercell size. We subsequently analyzed the pressure dependence of melting point and thus verified the Clausius–Clapeyron relationship. Furthermore, considering high temperature and irradiation, the effect of Shottky defects on melting point was investigated.

2. Molecular dynamics simulation for melting point

2.1. Interatomic potential function

In the present study, two types of potential function were used [9,10,12]. Both Eqs. (1) and (2) represent the Born–Mayer–Huggins

* Corresponding author. Tel./fax: +81 92 802 3494.
E-mail address: arima@nucl.kyushu-u.ac.jp (T. Arima).

0022-3115/$ - see front matter © 2009 Elsevier B.V. All rights reserved.
doi:10.1016/j.jnucmat.2009.01.020

type potential with the partially ionic model and include the Morse potential for the short-range interaction of the U–O covalent bond. There is, however, a difference in parameterization for the short-rage repulsive force. For evaluating many thermophysical properties of actinide oxides, Eq. (1) has been used so far [6–11]. The potential function proposed by Basak et al. [9] as a representative from Eq. (1) was used to evaluate the melting point here, and it referred to that proposed by Yamada et al. [6]. Eq. (1) from which Morse term was subtracted was the potential function proposed by Arima et al. [10]. The potential function expressed in Eq. (2) was more recently proposed by Yakub et al. [12], and it referred to both potential functions proposed by Basak et al. [9] and Yamada et al. [6].

$$U(r) = \frac{z_i z_j e^2}{r} + f_0(b_i + b_j)\exp\left(\frac{a_i + a_j - r}{b_i + b_j}\right) - \frac{c_i c_j}{r^6} + D_{ij}\{[\exp(-\beta_{ij}(r - r_{ij}^*)) - 1]^2 - 1\} \quad (1)$$

$$U(r) = \frac{z_i z_j e^2}{r} + A_{ij}\exp\left(-\frac{r}{\rho_{ij}}\right) - \frac{C_{ij}}{r^6} + D_{ij}\{[\exp(-\beta_{ij}(r - r_{ij}^*)) - 1]^2 - 1\} \quad (2)$$

Table 1
Potential parameters of UO_2 crystal in Eqs. (1) and (2).

	Basak et al. [9]	Arima et al. [10,18]		Yakub et al. [12]
ζ	0.6	0.675	ζ	0.5552
f_0 [eV Å^{-1}]	0.0422	0.0434		
O ion			O–O pair	
a [Å]	1.91	1.847	A [eV]	883.12
b [Å]	0.163511	0.166	ρ [Å]	0.3422
c [eV$^{1/2}$.Å^3]	1.987	4.166	C [eV Å^6]	3.996
U ion			U–U pair	
a [Å]	1.63	1.318	A [eV]	187.03
b [Å]	0.163511	0.036	ρ [Å]	0.3422
c [eV$^{1/2}$.Å^3]	0	0	C [eV Å^6]	0
U–O pair			U–O pair	
			A [eV]	432.18
			ρ [Å]	0.3422
			C [eV Å^6]	0
D [eV]	0.57745		D [eV]	0.5055
β [Å^{-1}]	1.65		β [Å^{-1}]	1.864
r^* [Å]	2.369		r* [Å]	2.378

where r is the distance between i and j atoms, and z_i is the ionic charge of the ith atom in the simulation, which is the product of the formal charge and the ionicity ζ. For example, the ionic charge of U for Basak potential is +4 × 0.6 = +2.4. In Eq. (1), f_0 is the fitting parameter for Basak potential and is the adjustable parameter (= 4.186 J Å^{-1} mol^{-1}) for Arima potential. Other potential parameters, a_i, b_i, c_i, D_{ij}, β_{ij}, r_{ij}^* in Eq. (1) and A_{ij}, ρ_{ij}, C_{ij}, D_{ij}, β_{ij}, r_{ij}^* in Eq. (2), were also determined based on experimental data, e.g., thermal expansion and compressibility. Details for the procedure to determine the potential parameters are found in Refs. [6–12,18]. Potential parameters mentioned above are summarized in Table 1.

In order to clarify the difference among these potential functions, the interaction energy as a function of r between ions and the thermal expansion of UO_2 in the solid phase are depicted in Figs. 1 and 2, respectively. As shown in Fig. 1(a), there is not so much difference in O–O interaction. For U–U interaction, the Coulomb repulsive energy dominates. The higher ionicity of U ion, the higher repulsive energy can be found in Fig. 1(b). In contrast, for U–O interaction the higher ionicity of O and U ions, the higher cohesive energy generates, as shown in Fig. 1(c). However, not only Coulomb interaction (attractive) but the short-range interactions (repulsive + attractive) contribute largely to U–O interaction. Fig. 2 shows the thermal expansion of UO_2 [19,20]. Every potential function reproduces well the thermal expansion from 300 to 2500 K. At the highest temperature (3000 K), Yakub potential gives a value comparable to the experimental one [20], and other potential functions give smaller values, which may result from the degree of ionicity.

2.2. Simulation technique for melting point

In the present study, all calculations were performed by MXDORTO and MXDORTOP programs. These original programs were developed by Kawamura and Hirao [21]. We made some alterations on them to use Basak and Yakub potential functions. The MXDORTOP program was prepared to run under the parallel computing system with the message passing interface (MPI) library. Since the Coulomb potential contributes to the cohesive energy of the UO_2 system, the calculation of Ewald summation is needed for such an ionic crystal. Recently, the Ewald scheme has

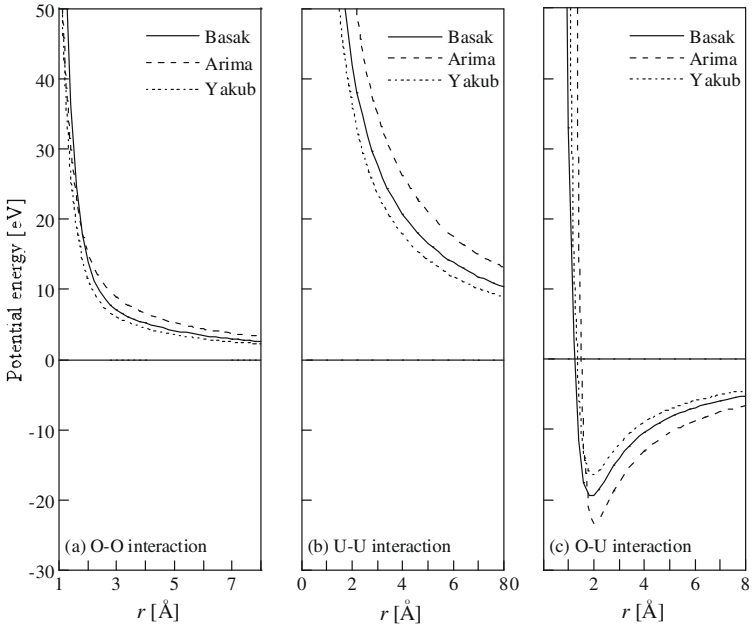

Fig. 1. Potential energies for the interaction of (a) O–O; (b) U–U; and (c) O–U. Potential functions were proposed by Basak et al. [9], Arima et al. [10] and Yakub et al. [12].

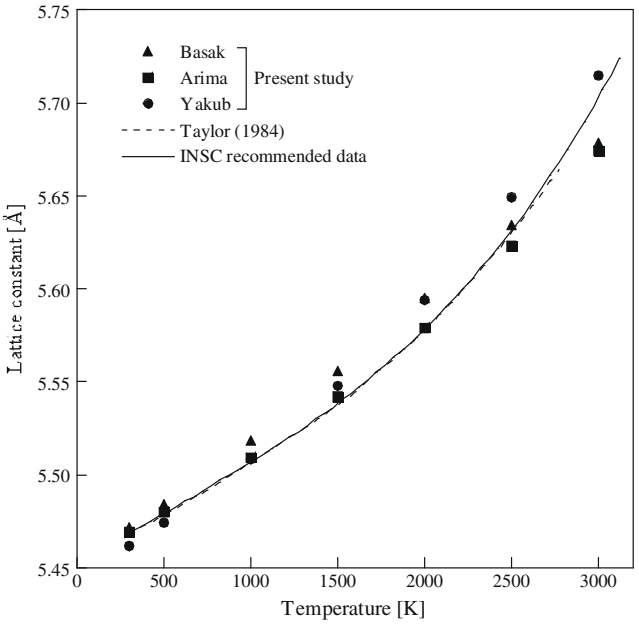

Fig. 2. Comparison of thermal expansions of UO_2 among the potential functions. MD calculations were performed for $3 \times 3 \times 3$ fluorite unit cells. Experimental data were provided by Taylor [19] and recommended by INSC [20].

been modified in order to simulate large scale of molecular and crystal systems efficiently [22,23]. But, there are not any alterations on the Ewald scheme in MXDORTO and MXDORTOP programs.

Two types of MD simulation were tested for evaluation of melting point. One was the one-phase simulation (OPS), and the other was the two-phase simulation (TPS). For OPS, the supercell at the initial state was prepared as the crystalline solid, and the MD calculation was subsequently performed at desired temperature and pressure (*NPT* ensemble). After passing enough time for the system to reach the equilibrium state, a determination was made whether the system was liquid or still solid based on density and enthalpy of UO_2 and visual information of crystal structure [24]. MD calculations of OPS were performed for $3 \times 3 \times 3$ fluorite unit cells (324 atoms). On the other hand, for TPS, solid (crystalline) and liquid phases coexisted in the supercell at the initial state. Solid and liquid phases were equilibrated for 20000 steps (=40 ps) at 300 and 4000 K, respectively. Both cells of the same size were subsequently placed side-by-side as the initial supercell. For instance, Fig. 3 shows the supercell at the initial state for $8 \times 8 \times 8 \times 2$ unit cells for TPS. Here, the last digit of 2 in the cell size means number of phases. Following MD calculations were made according to the same procedure as OPS. Each cell size (solid or liquid) used in TPS was varied to a maximum of $10 \times 10 \times 10$ unit cells (12000 atoms).

The configuration of the initial supercell with Schottky defects was made as follows. Here, one Schottky defect pair consists of one uranium vacancy and two oxygen vacancies. One uranium ion was randomly removed from its sub-lattice site in the fluorite structure, and subsequently two nearest neighbor oxygens were removed. This procedure was repeated until the number of pairs of the Schottky defect reached the desired one. The solid and liquid cells of the initial supercell for TPS were thermally equilibrated independently, and MD calculations with Schottky defects were performed at desired temperature and pressure for the joining cell.

For all calculations to determine the melting point, we varied the desired temperature at intervals of 50 K. Therefore, the error of the melting point due to this procedure is naively estimated to

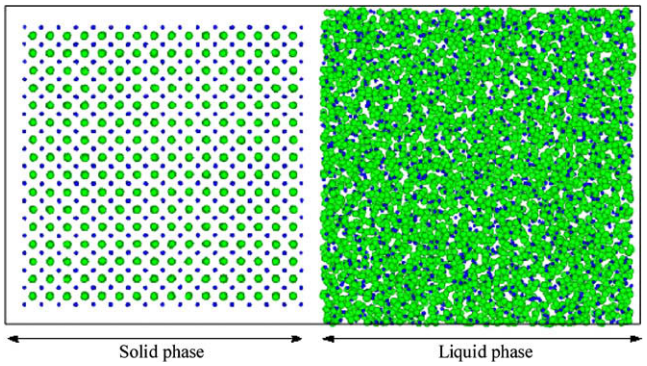

Fig. 3. Configuration of the supercell at the initial state of TPS with $8 \times 8 \times 8 \times 2$ unit cells (large ball: O ion; small ball: U ion). Left and right sides in the supercell were equilibrated at 300 and 4000 K, respectively. This picture was drawn by a 3D visualization program: VESTA [24].

be ±25 K, and the error bars corresponding to this value are plotted in figures concerning the melting point.

3. Results and discussion

3.1. Melting point and interatomic potential function

3.1.1. One-phase simulation (OPS)

Melting point calculations of OPS in the *NTP* ensemble were performed for the supercell of $3 \times 3 \times 3$ fluorite unit cells using Basak et al. [9], Arima et al. [10] and Yakub et al. [12] potentials. Densities of UO_2 as a function of temperature are shown in Fig. 4, together with experimental data [20,25–27]. It is found that each calculated density decreases gradually with an increase in temperature and drops steeply at melting point. Melting points ($T_{M.P.}$) obtained by Yakub, Basak and Arima potentials are 3625 ± 25,

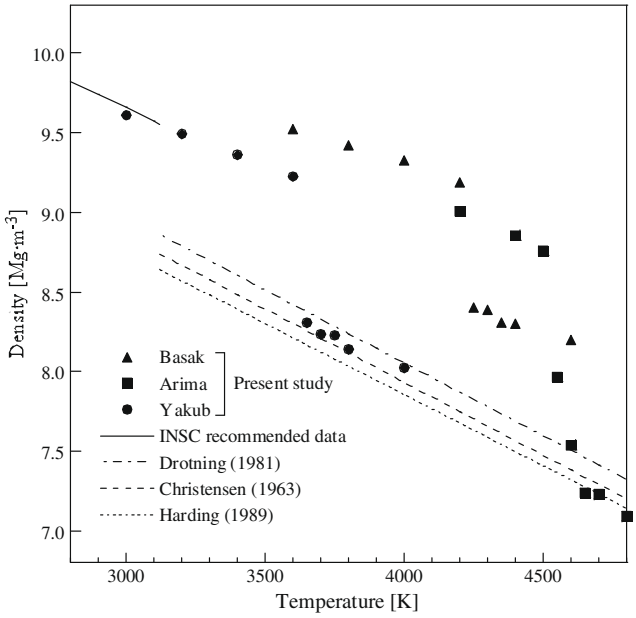

Fig. 4. Relationship between UO_2 density and temperature for OPS. MD calculations were performed for $3 \times 3 \times 3$ unit cells. Experimental data for the solid phase was recommended by INSC [20] and those of the liquid phase were given by Drotning [25], Christensen [26] and Harding et al. [27].

4225 ± 25 and 4550 ± 25 K, respectively. This result indicates that the melting point becomes higher with the degree of ionicity. In comparison with INSC recommended data of 3120 ± 30 K, the melting points obtained from OPS are found to be much higher. UO_2 densities obtained from Yakub potential from solid to liquid phases are, however, comparable to experimental data.

As described above, OPS gave a higher melting point than the experiment. In addition, OPS has a drawback, which is the solidification behavior. We performed OPS with Yakub potential according to the following simulation condition: the supercell was thermally equilibrated at 4000 K (liquid) and subsequently its temperature was gradually lowered to 300 K. The UO_2 thus obtained did not show the crystalline phase but the amorphous one. This situation was unlike the experimental one.

3.1.2. Two-phase simulation (TPS)

Firstly, we performed TPS in the *NTP* ensemble for the supercell consisting of solid and liquid phases where each cell size was $3 \times 3 \times 3$ unit cells. UO_2 densities obtained by TPS are shown in Fig. 5, together with experimental data [20,25–27]. TPS gives melting point of 3125 ± 25 K, 3325 ± 25 K and 3675 ± 25 K for Yakub, Basak and Arima potentials, respectively, and each melting point is much lower than that obtained from OPS. In addition, the melting point obtained from Yakub potential is comparable to INSC recommended data. This is due to the fact that the initial supercell of TPS has different phases of solid and liquid UO_2 at the initial state, and consequently the disorder in the liquid phase propagates easily to the solid phase in lower temperatures. On the contrary, the initial supercell of OPS does not contain the disorder phase which plays a role as a trigger for melting, which results in a too high calculated melting point. The relationships between the melting point and the potential function and between UO_2 density and temperature for TPS show a similar tendency with those for OPS.

Secondly, we investigated the dependence of melting point on the supercell size which varied from $3 \times 3 \times 3 \times 2$ to $10 \times 10 \times 10 \times 2$ unit cells using Yakub potential. The small supercell size is desirable for efficient calculation whereas the large size is better for precise calculation. The melting point was plotted as a function of the supercell size in Fig. 6. The result shows that the melting point increases slightly with the supercell size and one obtained for the largest cell was estimated to be 3175 ± 25 K. Therefore, a supercell size greater than $7 \times 7 \times 7 \times 2$ unit cells is enough to precisely estimate the melting point. For TPS with a supercell of $8 \times 8 \times 8 \times 2$ unit cells, the atomic configurations at 3150 and 3200 K are visually shown in Figs. 7 and 8, respectively. Fig. 7(a) shows a snapshot at 800 ps at 3150 K, and the solid phase expands into the liquid region. After 1200 ps, the supercell completely became solid (Fig. 7(b)). In contrast, at 3200 K, the liquid phase still grows at 120 ps in Fig. 8(a), and completely stabilizes at 200 ps in Fig. 8(b). As shown in Figs. 7 and 8, the time required to complete crystallization is much longer than that for melting, which predicts that in fact, the melting point is closer to 3150 K rather than 3200 K. Furthermore, crystallization and melting behaviors not observed in OPS have occurred in TPS.

One of the important thermodynamic properties regarding the melting behavior is the latent heat of melting (or heat of fusion).

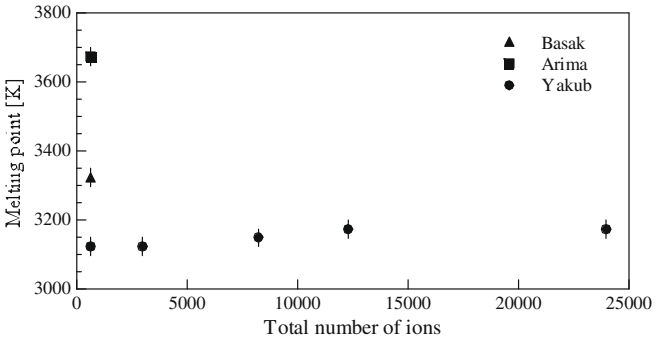

Fig. 6. Supercell size dependence of melting point. MD calculations were performed according to the procedure TPS.

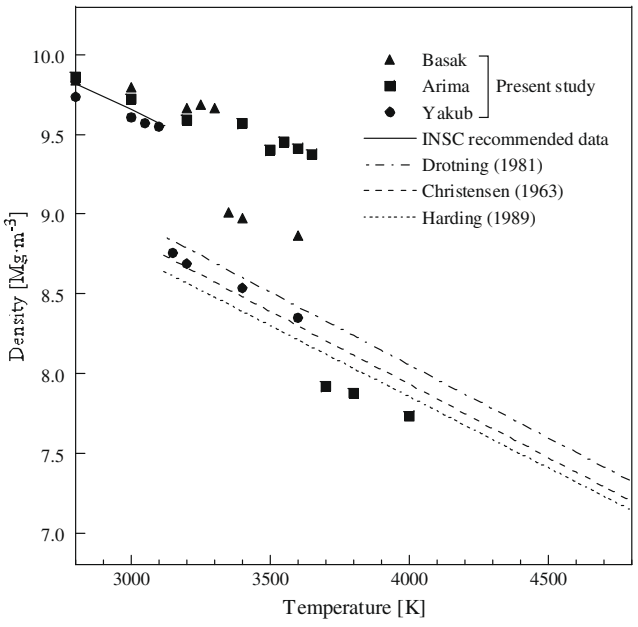

Fig. 5. Relationship between UO_2 density and temperature for TPS. MD calculations were performed for $3 \times 3 \times 3 \times 2$ unit cells. Literature data were the same as in Fig. 4.

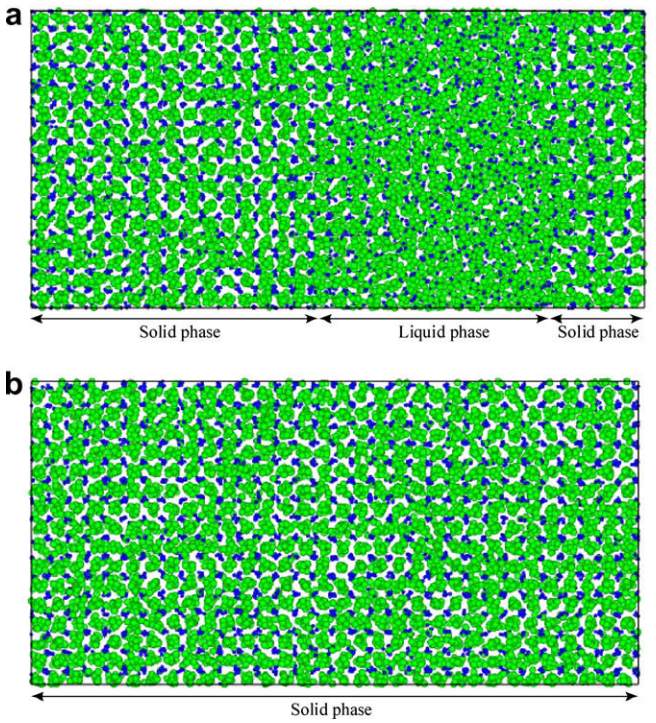

Fig. 7. Configurations of the supercells after (a) 800 ps; and (b) 1200 ps at 3150 K. TPS was performed for $8 \times 8 \times 8 \times 2$ unit cells. These pictures were drawn by VESTA [24].

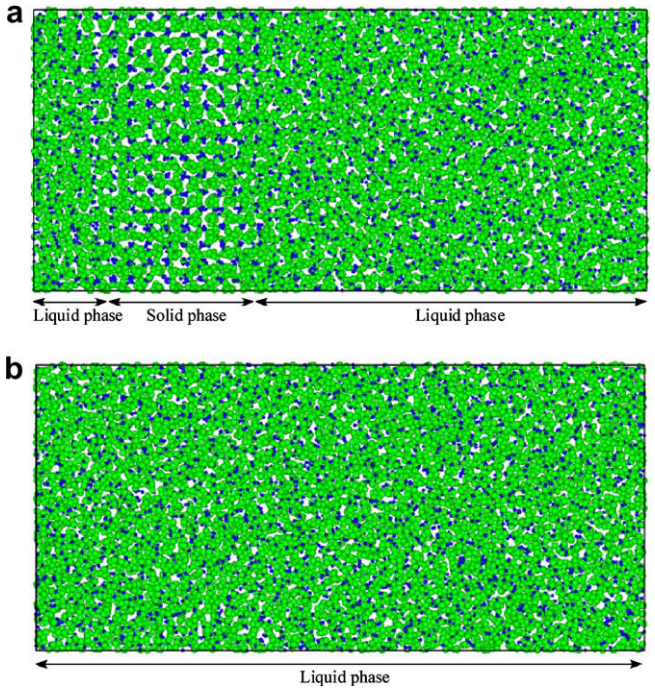

Fig. 8. Configurations of the supercells after (a) 120 ps; and (b) 200 ps at 3200 K. TPS was performed for $8 \times 8 \times 8 \times 2$ unit cells. These pictures were drawn by VESTA [24].

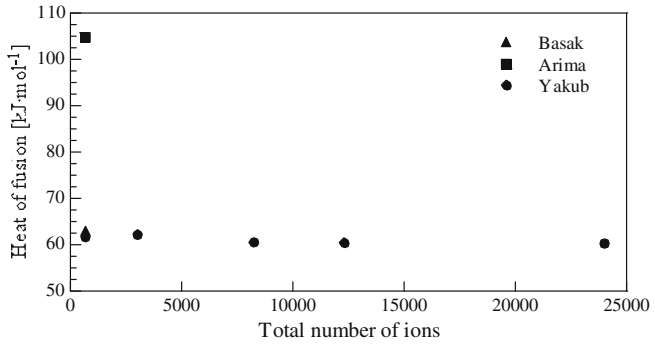

Fig. 9. Relationship between heat of fusion and supercell size. MD calculations were performed according to the procedure of TPS.

The heat of fusion is defined as the difference in enthalpy between solid and liquid phases in the vicinity of the melting point. Fig. 9 shows the heat of fusion, ΔH_{fusion}, as a function of the supercell size. The result shows that the heat of fusion is almost independent on the supercell size and is about 60 kJ mol^{-1} for Yakub potential and is a little smaller than INSC recommended value of 70 kJ mol^{-1} [20]. As shown in Fig. 9, Arima potential gives the largest value of ΔH_{fusion} for the smallest supercell, which may result in the highest melting point.

3.2. Dependence of melting point on pressure

The pressure dependence of melting point was investigated to clarify the phase boundary between solid and liquid UO_2. All calculations were performed in the *NPT* ensemble for $8 \times 8 \times 8 \times 2$ unit cells. The pressure was change from 0.1 to 3000 MPa. Fig. 10 shows that the melting point of UO_2 linearly increases with pressure applied to the system. As a result, TPS gave the relationship between melting point and pressure

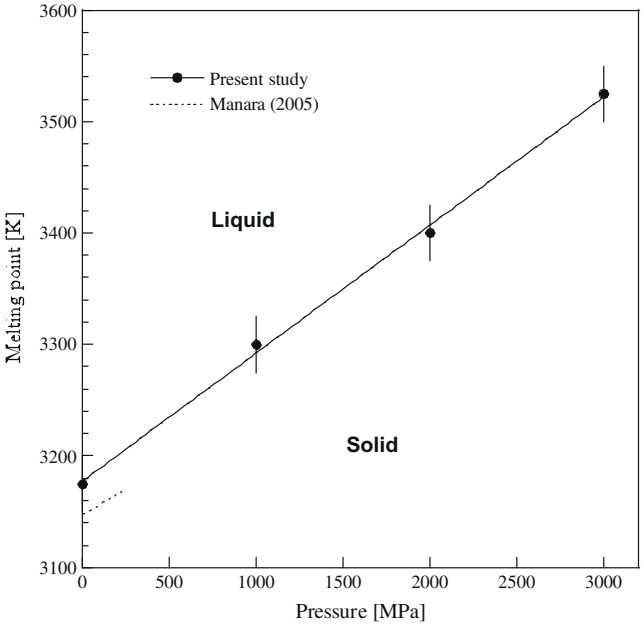

Fig. 10. Pressure dependence of melting point. MD calculations were performed for $8 \times 8 \times 8 \times 2$ unit cells. Experimental data was obtained from Ref. [2].

$$T_{\text{M.P.}}[\text{K}] = (3178 \pm 20) + (11.5 \pm 1.1) \times 10^{-2} p, \tag{3}$$

where p is pressure in MPa. Though it was very difficult to experimentally determine the melting point as a function of pressure, the experimental relationship between 10 MPa and 250 MPa was given by Manara et al. [2]: $T_{\text{M.P.}}$ [K] = 3147 + 9.29 × $10^{-2}p$. Both the melting point at 0 MPa and the slope of $dT_{\text{M.P.}}/dp$ obtained from TPS are a little larger than those experimentally obtained.

The relationship between melting point and pressure is given as the Clausius–Clapeyron equation by the classical thermodynamic theory as follows:

$$\frac{dT_{\text{M.P.}}}{dp} = \frac{T_{\text{M.P.}} \Delta V_{\text{m}}}{\Delta H_{\text{fusion}}}, \tag{4}$$

where ΔV_{m} is the change of molar volume on the melting point. The left side of Eq. (4) was already obtained from the relationship between melting point and pressure as shown in Eq. (3). The right side can be independently estimated based on the results obtained in Section 3.1.2. In order to precisely estimate it, we used the results obtained for the largest supercells ($8 \times 8 \times 8 \times 2$ and $10 \times 10 \times 10 \times 2$ unit cells). Thus, averaged ΔV_{m} and ΔH_{fusion} were 2.50×10^{-6} m^3 mol^{-1} and 60.38 kJ mol^{-1}, respectively. Consequently, the right side of Eq. (4) was estimated to be 13.13×10^{-2} K MPa^{-1}. These results are in reasonable agreement. So, the Clausius–Clapeyron relationship can be also maintained in MD simulations, which confirms that MD simulations performed in this work are thermodynamically consistent.

3.3. Effect of Schottky defects

The effect of Schottky defects on melting point was investigated by TPS. As described in Section 2.2, the Schottky defect consisted of one uranium vacancy and two nearest neighbor oxygen vacancies in the present study. A maximum of 150 pairs of Shottky defects was introduced into a $8 \times 8 \times 8$ unit cells. Considering the formation energy of a Shottky defect for UO_2 (ca. 5.6–7 eV [28,29]), the concentrations of uranium and oxygen vacancies might be too high. In future, we will discuss the effect of Xe on the melting point, and such lattice defects, e.g., fission products, vacancies

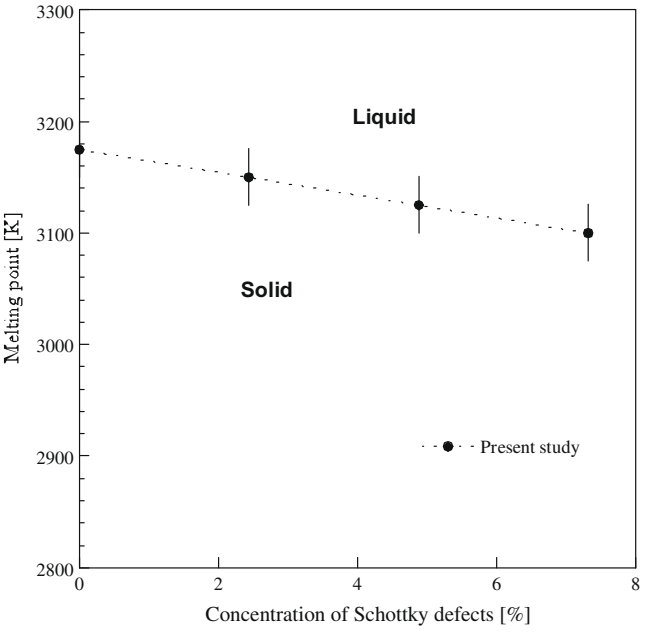

Fig. 11. Dependence of melting point on the concentration of Schottky defects. MD calculations were performed for $8 \times 8 \times 8 \times 2$ unit cells.

and so on, may be found in large quantities under high irradiation, especially in the rim region of UO_2 fuels [30,31]. It is shown in Fig. 11 that the melting point of UO_2 decreases with an increase of the concentration of Schottky defects. Kurosawa pointed out that the melting of ionic crystals was attributed to lattice defects as well as lattice vibrations [32]. Therefore, the Schottky defect which locally disordered the crystallinity caused lowering of the melting point.

4. Conclusions

MD simulations have been applied to evaluate the melting point of UO_2 using the interatomic potential functions proposed by Basak, Arima and Yakub. These potentials have a similar function form, however, there are differences in the degree of ionicity and in the short-range potential. In addition, two types of simulations were performed in the present study. The first one is the one-phase simulation (OPS) for which MD calculations started from a homogeneous solid phase. The second one is a two-phase simulation (TPS) whose initial supercell consists of solid and liquid phases. Regarding to the simulation technique to determine the melting point, TPS gave much lower melting point than OPS for each potential function, and closer to experimental data, which indicates that the disordered phase existing as liquid in the initial state played a role of a trigger for melting. The melting point given by Yakub potential was the lowest for both OPS and TPS and comparable to experimental data for TPS, which might result from its low ionicity. As well as the melting point, the heat of fusion was obtained as a function of supercell size. Then we evaluated the pressure dependence of melting point between 0.1 and 3000 MPa. The result showed that the first derivative of the melting point with respect to pressure, which was obtained by MD calculations, was a little larger than the literature data. Evaluating the heat of fusion and the pressure dependence of melting point separately, the Clausius–Clapyeron equation could be verified, confirming the thermodynamic consistency of our calculations. Furthermore, MD simulations showed the result that the melting point decreases with the increase of the concentration of Schottky defects, which resulted from that the local disorder generated by the Schottky defect helped to melt the UO_2 crystal.

Acknowledgment

The authors would like to thank K. Kawamura for usage of the MXDORTO and MXDORTOP programs.

References

[1] M. Kinoshita, T. Kameyama, S. Kitajima, Hj. Matzke, J. Nucl. Mater. 252 (1998) 71.
[2] D. Manara, C. Ronchi, M. Sheindlin, M. Lewis, M. Brykin, J. Nucl. Mater. 342 (2005) 148.
[3] M.G. Adamson, E.A. Aitken, R.W. Caputi, J. Nucl. Mater. 130 (1985) 349.
[4] M. Kato, K. Morimoto, H. Sugata, K. Konashi, M. Kashimura, T. Abe, J. Nucl. Mater. 373 (2008) 237.
[5] S. Motoyama, Y. Ichikawa, Y. Hiwatari, A. Oe, Phys. Rev. B 60 (1999) 292.
[6] K. Yamada, K. Kurosaki, M. Uno, S. Yamanaka, J. Alloys. Compd. 307 (2000) 1.
[7] K. Yamada, K. Kurosaki, M. Uno, S. Yamanaka, J. Alloys. Compd. 307 (2000) 10.
[8] K. Kurosaki, K. Yamada, M. Uno, S. Yamanaka, K. Yamamoto, T. Namekawa, J. Nucl. Mater. 294 (2001) 160.
[9] C.B. Basak, A.K. Sengupta, H.S. Kamath, J. Nucl. Mater. 360 (2003) 210.
[10] T. Arima, S. Yamasaki, Y. Inagaki, K. Idemitsu, J. Alloys. Compd. 400 (2005) 43.
[11] T. Arima, S. Yamasaki, Y. Inagaki, K. Idemitsu, J. Alloys. Compd. 415 (2006) 43.
[12] E. Yakub, C. Ronchi, D. Staicu, J. Chem. Phys. 127 (2007) 094508.
[13] K. Govers, S. Lemehov, M. Hou, M. Verwerft, J. Nucl. Mater. 366 (2007) 161.
[14] K. Govers, S. Lemehov, M. Hou, M. Verwerft, J. Nucl. Mater. 376 (2008) 66.
[15] A.B. Belonoshko, L.S. Dubrovinsky, Geochim. Cosmochim. Acta 59 (1995) 1883.
[16] K. Harafuji, T. Tsuchiya, K. Kawamura, J. Appl. Phys. 96 (2004) 2501.
[17] T. Karakasidis, P.J.D. Lindan, J. Phys.: Condens. Mater. 6 (1994) 2965.
[18] H. Inaba, R. Sagawa, H. Hayashi, K. Kawamura, Solid State Ion. 122 (1999) 95.
[19] D. Taylor, Br. Ceram. Trans. J. 83 (1984) 32.
[20] International Nuclear Safety Centre (INSC), Material Properties Database, Argonne National Laboratory, Illinois, USA, http://www.insc.anl.gov/matprop/.
[21] K. Hirao, K. Kawamura, Material Design Using Personal Computer, Shokabo, Tokyo, 1994.
[22] D. Wolf, P. Keblinski, S.R. Phillpot, J. Eggebrecht, J. Chem. Phys. 110 (1999) 8254.
[23] E. Yakub, C. Ronchi, J. Chem. Phys. 119 (2003) 11556.
[24] K. Momma, F. Izumi, J. Appl. Crystallogr. 41 (2008) 653.
[25] W.D. Drotning, in: Proceedings of the 8th Symposium on Thermophysical Properties, National Bureau of Standard, Gaithersburg, Maryland, June 15–18, 1981.
[26] J.A. Christensen, J. Am. Ceram. Soc. 46 (1963) 607.
[27] J.H. Harding, D.G. Martin, P.E. Potter, Commission of European Communities Report EUR 12402, 1989.
[28] Hj. Matzke, J. Chem. Soc., Farad. Trans. II 83 (1987) 1121.
[29] M. Freyss, T. Petit, J.P. Crocombette, J. Nucl. Mater. 347 (2005) 44.
[30] R.A. Jackson, C.R.A. Catlow, J. Nucl. Mater. 127 (1985) 161.
[31] H.Y. Geng, Y. Chen, K. Kaneta, M. Kinoshita, J. Alloys. Compd. 457 (2008) 465.
[32] T. Kurosawa, J. Phys. Soc. Jpn. 12 (1957) 338.